ROYAL SOCIETY OF CHEMISTRY

Chem Soc Rev

Taming molecular collisions by electric and magnetic fields

SCHOLARONE™
Manuscripts

ARTICLE TYPE

Taming molecular collisions using electric and magnetic fields

Mark Brouard,[a] **David H. Parker,**[b] **and Sebastiaan Y.T. van de Meerakker**[b‡]

The motion of molecules that possess a permanent electric or magnetic dipole moment can be manipulated using electric or magnetic fields. Various devices have been developed over the last decades to deflect or focus molecules, to orient them in space, and to decelerate or accelerate them. These precisely controlled molecules are ideal starting points for scattering experiments that reveal the quantum mechanical nature of molecular interactions. In this Tutorial Review, we present an overview of the various manipulation tools, discuss how they can be used to advantage in molecular beam scattering experiments, and review recent progress in this field. We describe a selection of benchmark experiments that illustrate the unique possibilities that are available nowadays to study molecular collisions under controlled conditions.

1 Introduction

Molecular change - the basis of chemistry - takes place via interaction of molecules with light, ions, or with other molecules. The key to understanding molecular change is to characterize the conditions before, during, and after change occurs in as much detail as possible. In our efforts to understand molecular change taking place via collisions of molecules with other molecules, a proven approach is to 'tame' or control molecules before they collide, using sophisticated molecular beam methods and electric or magnetic fields. Stern and Gerlach provided an early and spectacular example of beam manipulation in 1922 by directing a molecular beam of silver atoms through an inhomogeneous magnetic field[1]. Their result, an image of the downstream beam on a photographic plate, provided the first confirmation of space quantization of electron spin. Since then, progress in our understanding of molecular properties and chemical change has advanced in periods of great activity spaced by quiet interludes, an early one due to World War II, but more often due to shortcomings in the last turn of the key – our ability to determine the results of molecular change.

Indeed, progress in 'taming' molecular degrees of freedom went hand in hand with progress in developing the methods to detect them. In the early experiments, static electric or magnetic fields were placed in the region between the molecular beam sources and the scattering center to define the initial conditions, as well as between the scattering center and

detector for product state specification. This approach was followed first in the early 1950s by Townes and coworkers[2] and independently by Paul and coworkers[3], where an electric quadrupole field was used to focus specific states of a diverging molecular beam back to the beam axis. This made sensitive collision studies of state-selected molecules feasible due to the increased number density of the molecules. In 1961 Toennies used a set of tandem electrostatic quadrupoles before and after a scattering cell to measure collision-induced integral state-to-state cross sections for rotational inelastic scattering of thallium fluoride molecules with a variety of target atoms and molecules[4]. State selection and subsequent orientation of molecules in a strong electric field were combined in 1964 by Toennies, Paul, and coworkers[5] to measure the angle-dependencies of intermolecular potentials using preferentially oriented molecules. This led in 1966 to a series of direct measurements of the steric effect for chemical reactions by the groups of Brooks[6] and Bernstein[7], often using reactions of alkali metals with oriented symmetric top molecules, such as methyl iodide. The most sophisticated of these experiments were able to determine the dependence of the angular distributions of the scattered products, or the differential cross section, on methyl iodide C–I bond-axis orientation[8]. As a result, the authors were able to provide direct experimental evidence in support of the 'cone-of-acceptance' model of chemical reactivity, which reflects a dependence of the reaction barrier to angle of attack.

In the 80's and 90's new types of experiments emerged due to the advent of laser-based detection methods such as resonance enhanced multi-photon ionization (REMPI) or laser induced fluorescence (LIF)[9]. This enabled measurements of full state-to-state integral and differential cross sections, as well as vector correlations between pre- and post-collision parameters. In the past decade, new and improved molecular ma-

[a] *The Department of Chemistry, University of Oxford, The Physical and Theoretical Chemistry Laboratory, South Parks Road, Oxford OX1 3QZ, United Kingdom*
[b] *Radboud University Nijmegen, Institute for Molecules and Materials, Heijendaalseweg 135, 6525 AJ Nijmegen, the Netherlands*
‡ To whom correspondence should be addressed. E-mail: basvdm@science.ru.nl

nipulation and detection techniques have stimulated another surge of activity in the field, bringing us at this moment to a nearly perfect understanding of molecular change. Perfection, however, is still limited to a handful of the very simplest molecular systems. Recent progress in expanding this level of understanding towards larger systems is also addressed in this review.

We review studies of molecular change carried out under single collision conditions in the gas-phase, and focus primarily on molecules tamed before collision by the combination of molecular beams and electric or magnetic fields. This narrow scope includes many exciting recent advances in our field, as highlighted in this text. In this Tutorial Review, we start in section 2 by introducing a few general concepts on molecular scattering in order to appreciate the advantages of 'taming' the collision. We will describe the reward for controlling collisions – a beautifully simple and symmetric sphere – and define the molecular properties that need to be characterized and controlled in order to reveal this (in honor of Sir Isaac) 'Newton' sphere for a simple inelastic collision system. Next, a short perspective on experiments leading to the current state-of-art will be given, stressing again the important role of product detection. This theme mirrors the delightful Noble prize speech of Dudley Herschbach (1986) who distinguished three eras of progress in molecular beam research as the 'alkali' era – based on detection of species with a low ionization potential by a hot filament; the 'universal' era – using electron impact- and (more recently) photo- ionization detection; and finally (in 1986) the 'laser-based' era – including laser induced fluorescence and ionization. Nowadays, the dividing lines are less simple, and, furthermore, the label 'era' could suggest extinction, which is certainly not the case.

In section 3 we give a brief introduction to the interaction of molecules with electric and magnetic fields, that forms the basis for all manipulation tools described in this Review. We then present a series of sections that each focuses on controlling a certain molecular degreee of freedom. In section 4, methods are described to select the internal quantum states of molecules. These include the selection of specific rotational states for diatomic molecules and conformers for larger polyatomic molecules. The possibilities to orient the bond axis of molecules in space are discussed in section 5. Methods to control the velocity of molecules using techniques akin to charged particle accelerators are highlighted in section 6. We dedicate section 7 to the study of molecular collisions at low collision energies; a young and rapidly developing field in which the manipulation tools described here can play an important role. Each section starts with a brief explanation of the operation principles of the tools available to control the degree of freedom.

We are not exhaustive in the description of all manipulation tools and devices themselves, as this has been thoroughly re-viewed recently [10]. Neither will we present a complete review on all collision experiments that have made use of electric and magnetic manipulations tools. For this, the field is too large and has too many practitioners to be covered here. Instead, we describe a selection of recent benchmark experiments that illustrate how these tools can be implemented in collision experiments, and we discuss what they can offer to unravel the fundamental mechanisms of molecular interactions. Where appropriate, references are given to reviews that present a more complete overview of the field. We exclusively focus on electric and magnetic field manipulation of neutral molecules in gas-phase collision experiments; surface scattering and the manipulation of molecules using optical fields is beyond the scope of this Tutorial Review.

2 General concepts

Consider a generic $(A + B \rightarrow A' + B')$ bimolecular inelastic collision system where A and B exchange rotational or vibrational energy, and in which all species are in well-defined quantum states. Upon a collision, the recoil directions of A' and B' will deviate from the A, B initial directions, as shown schematically in Figure 1. When the inelastic collision shows forward scattering, typical for low amounts of energy exchange, the recoil directions deviate only slightly from the initial directions. If the initial conditions are constant, A' and B' must always end up somewhere on the surface of a pair of well-defined velocity spheres. The exact positions on the surfaces cannot be predicted because we are still unable to control the relative distance between A and B at collision, but the surface pattern on the Newton sphere provides sufficient information to unravel this distance dependence. In this way the intermolecular potential energy surface, which determines the forces governing all aspects of the molecule-molecule interaction, is determined.

In an 'untamed' collision experiment with a wide range of initial states, collision energies, mutual orientations, and undefined final states, the spheres are no longer distinguishable and critical information is lost. In this review we will discuss a variety of methods that are available nowadays to precisely control the initial conditions, i.e., quantum state, collision energy, and orientation. Yet, this in itself is not sufficient to unravel the scattering dynamics. Equally important is the ability to capture the information encoded on each product state Newton sphere. For this, detection methods are required that probe the product molecules state-selectively, sensitively, and as a function of the scattering angle θ.

The solution has evolved since the beginning of crossed-beam molecular beam scattering, and is based on the general concepts illustrated in Fig. 2a. Following crossed-beam scattering with state-selected reactants, a single product-state Newton sphere expands at its fixed recoil velocity while the
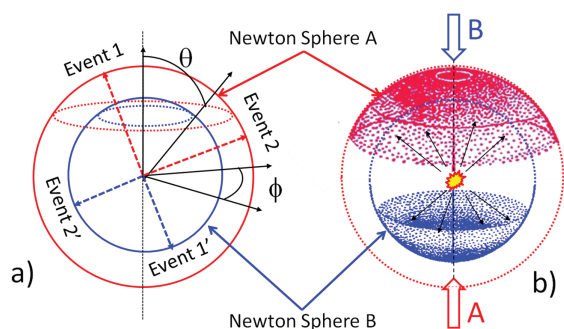
Fig. 1 Newton spheres in the center-of-mass frame for inelastic scattering in the forward direction. By defining the energy of the collision, conservation of energy and momentum determines the velocity of the final products A and B, (mass B > mass A) which recoil in opposite directions. In the center-of-mass frame there is cylindrical symmetry about the azimuthal angle ϕ (defined in panel a). Two events are shown, by repeating the experiment under identical conditions, a sphere of products emerges (b) where the surface pattern on the sphere reveals the dynamics of the scattering process.

full ensemble of products moves at the center-of-mass velocity. With neutral product time-of-flight (TOF) detection methods (e.g., hot-wire, universal, and the more recent H-atom Rydberg tagging), Fig 2b, the detector is rotated around the scattering plane and intercepts small patches (front and back) of the product Newton sphere. Measurements are made for each laboratory detection angle and a laboratory-frame to center-of-mass transformation is necessary in order to construct the center-of-mass frame Newton sphere. From the recorded TOF, the product recoil velocity and internal quantum state can be deduced. The ultimate goal is to measure the surface pattern of the state-to-state Newton sphere. If the scattering process is axially symmetric, a slice through the center of the Newton sphere in the scattering plane, Fig. 2b, contains all relevant information; this slice of signal intensity as a function of scattering angle θ (θ defined in fig 1a) is called the state-to-state differential cross-section (DCS). The DCS is integrated over θ to yield the state-to-state integral cross section.

With the advent of modern laser-based detection techniques such as REMPI and LIF, extremely sensitive and state-selective detection of product molecules has become possible. In scattering experiments, the detection laser is directed through the beam crossing area, probing directly the number of product molecules in a given quantum state within the laser probe volume. With REMPI, the laser is used to convert neutral scattering products into ions which are then projected into a TOF region by an electric field and mass-selected at the detector by their time-of-arrival. With LIF, the laser is used to
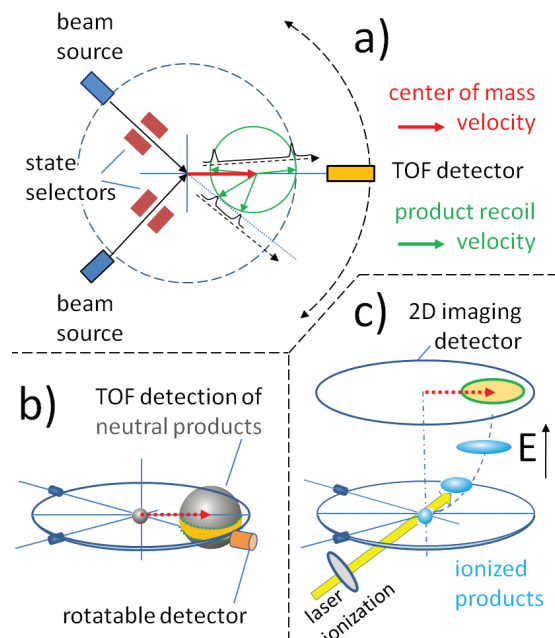
Fig. 2 Two types of product detection in a crossed-beam scattering experiment using state-selected initial states. *a* Equatorial slice through a Newton Sphere (green circle) produced in the laboratory frame by crossed molecular beam scattering. A time-of-flight detector positioned at different scattering angles measures the time dependence of the arriving signal, which is the vector sum of the product recoil velocity (center-of-mass frame) and the center-of-mass velocity in the scattering plane of the two molecular beams. *b* Detection of a small solid angle of the three-dimensional neutral Newton sphere when it reaches the detector. *c* Imaging detection uses laser ionization (such as resonance enhanced multiphoton ionization, REMPI) to convert the entire neutral Newton sphere to an ionic Newton sphere at the crossing point. The ion sphere is then projected by a special velocity mapping electrostatic (E) field and crushed onto a two-dimensional (2-D) imaging detector. By adjusting the E field it is also possible to detect only the center 'slice' of the product Newton sphere.

excite product molecules to a short-lived electronically excited state. The emitted photons are then collected and registered using light detectors.

For both methods, even energetically near-degenerate final states can often be probed individually by exploiting the selection rules for optical transitions. This allows for measurements of integral state-to-state scattering cross sections at the full (hyper)fine structure level. Unfortunately, however, the angular distribution of the scattering products is not measured using these methods, although information on the product recoil velocity can be extracted from the Doppler profiles of the optical transitions used.

The ability to capture information on the Newton sphere in crossed beam scattering took a major leap forward by the development of laser-based ion imaging[11] methods such as velocity map imaging (VMI)[12], see Figure 2c. In these methods, the neutral Newton sphere is converted into an ionic Newton sphere at the crossing point using REMPI. The ion sphere is then projected and imaged by an electrostatic (E) field and 'crushed' onto a two-dimensional (2-D) charged particle detector, where it is recorded on a multi-anode collector or on a phosphor screen monitored by a camera system. Velocity map imaging (VMI) is probably the most advanced detection technique available nowadays in collision experiments, as it combines sensitive state-selective detection of product molecules with efficient probing of the Newton sphere.

3 Electric and magnetic fields: controlling molecular motion

Molecules that possess an electric or magnetic dipole moment are influenced by the presence of an externally applied electric or magnetic field, respectively. The dipole moment couples to the external field, resulting in a shifting and splitting of the energy levels. In case of electric and magnetic fields, we refer to this as the Stark and Zeeman effect, respectively. The Stark and Zeeman energies are forms of potential energy of the molecule. If the field is homogeneous, this energy is simply added to the internal energy of the molecule. If, however, the field is inhomogeneous, a force $\vec{F}(\vec{r}) = -\vec{\nabla} U(\vec{r})$ on the molecule is exerted, where $U(\vec{r})$ is the Stark or Zeeman energy as a function of the position $\vec{r}$. It is this force that is used throughout in the manipulation tools described in this Tutorial Review. When applied correctly, it provides the handle needed to control both the internal (quantum state) and external (laboratory orientation or velocity) degrees of freedom of molecules.

The calculation of the Stark or Zeeman energies of rovibrational levels of a molecule can be a difficult task, and requires detailed knowledge of the energy level structure of the molecule. A full description is beyond the scope of this Tuto-
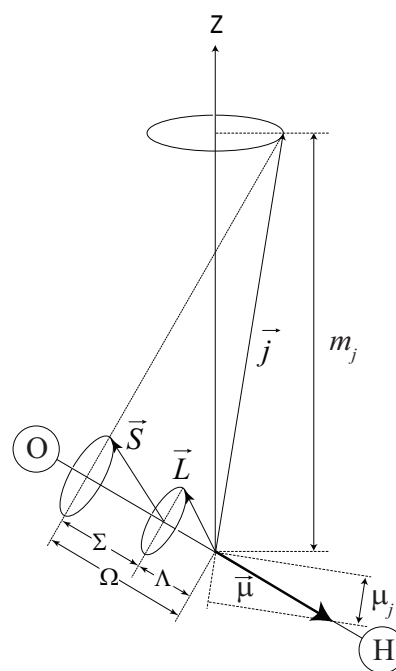
Fig. 3 Vector diagram of the relevant angular momenta of a diatomic molecule, such as OH (X), in the presence of an electric field. The field is directed along the Z-axis. See text for details.

rial Review; a more detailed description and a formal quantum mechanical derivation of the formalism is found in Ref[10] and references therein. We here restrict ourselves to a description of the most basic ingredients using a simple yet instructive vector diagram[10] as shown in Figure 3. We will use the OH radical as an example, as this species possesses both an electric and magnetic dipole moment, and is frequently used in collision experiments.

Let us start with the Stark effect. The Hamiltonian describing the interaction between the electric dipole moment $\vec{\mu}$ of a molecule and an electric field $\vec{E}$ is given by

$$H_{\text{Stark}} = -\vec{\mu} \cdot \vec{E} = -\mu E \cos \theta. \tag{1}$$

The angle θ describes the angle between the dipole moment of the molecule, which for a diatomic molecule is directed along the bond axis, and the externally applied electric field. The difficulty in calculating the Stark energies arises from the fact that the dipole moment is defined in the (rotating!) molecular frame, whereas the electric field axis is defined in the laboratory frame.

Quantum mechanics dictates that in the presence of an electric or magnetic field, the total angular momentum $\vec{j}$ of a molecule can have only certain discrete orientations with respect to the field axis. The component of $\vec{j}$ on the field axis is given by $\hbar m_j$. The quantum number m_j is for historical reasons often referred to as the magnetic quantum number, and

can take the values $-j, -j+1, ..., j$. The magnitude of the total angular momentum vector is given by $\hbar\sqrt{j(j+1)}$, and this quantity is in first order conserved in the presence of a field. Instead, a precession of $\vec{j}$ around the field axis takes place at an angle whose cosine is given by $m_j/\sqrt{j(j+1)}$.

The projection of $\vec{j}$ onto the bond axis of the molecule is also conserved, and takes the value $\hbar\Omega$. The quantum number Ω labels the spin-orbit state of the molecule, and represents the coupling of the orbital $\vec{L}$ and spin $\vec{S}$ angular momenta of the electrons, whose projections on the bond axis are given by Λ and Σ, respectively. For OH ($X\,^2\Pi$), $|\Omega|$ can take the values 1/2 and 3/2. Each value for Ω represents a different rotational level $|j\Omega\rangle$ of the molecule. As the molecule rotates, nutation of the bond axis around $\vec{j}$ occurs at an angle whose cosine is given by $\Omega/\sqrt{j(j+1)}$.

The projection of $\vec{\mu}$ onto $\vec{E}$ is now established as follows. We first calculate the projection μ_j of $\vec{\mu}$ on $\vec{j}$, and then the projection of μ_j onto the external field axis. It then follows that the projection of $\vec{\mu}$ onto $\vec{E}$ is given by $\mu m_j/\sqrt{j(j+1)} \cdot \Omega/\sqrt{j(j+1)}$. Hence, to first order, the Stark energy U_{Stark} for a rotational state $|j\Omega\rangle$ is given by

$$U_{\text{Stark}} = -\frac{m_j\Omega}{j(j+1)}\mu E. \qquad (2)$$

For the $j = 3/2$ rotational ground state of OH ($X\,^2\Pi_{3/2}$), Ω can take the values $-3/2$ and $3/2$, and m_j can take the values $-3/2, -1/2, 1/2$ and $3/2$. As will be discussed in more detail in section 4.1, each rotation state of molecules in a $^2\Pi$ electronic state is split into two closely separated Λ-doublet levels, usually labelled e and f, which define the total parity of the diatomic (see, for instance, the energy level diagram of OH in the upper panel of Figure 6). Here, $\varepsilon = \pm 1$ denotes whether the wavefunction is written as symmetric ($\varepsilon = +1$) or anti-symmetric ($\varepsilon = -1$) linear combinations of $|j\Omega\rangle$ and $|j-\Omega\rangle$, whereas the total parity p is given by $p = \varepsilon(-1)^{j-1/2}$. For OH ($X$) this Λ-doublet splitting amounts to $E_\Lambda = 0.055$ cm^{-1}. A proper quantum mechanical treatment of the Stark effect [10] reveals that in the presence of an electric field both levels mix into a superposition of both parity levels. For the ($X\,^2\Pi_{3/2}, j = 3/2$) state of OH, equation 2 is then modified into

$$U_{\text{Stark}} = \frac{E_\Lambda}{2} \pm \sqrt{\left(\frac{E_\Lambda}{2}\right)^2 + \left(\mu E \frac{m_j\Omega}{j(j+1)}\right)^2}, \qquad (3)$$

where the $+$ and $-$ sign must be chosen for molecules in the upper and lower Λ-doublet component, respectively. Consequently, molecules in the upper component gain Stark energy in increasing electric fields, whereas the energy for molecules in the lower component is reduced. Levels that belong to the f and e components are therefore called 'low-field-seeking' and
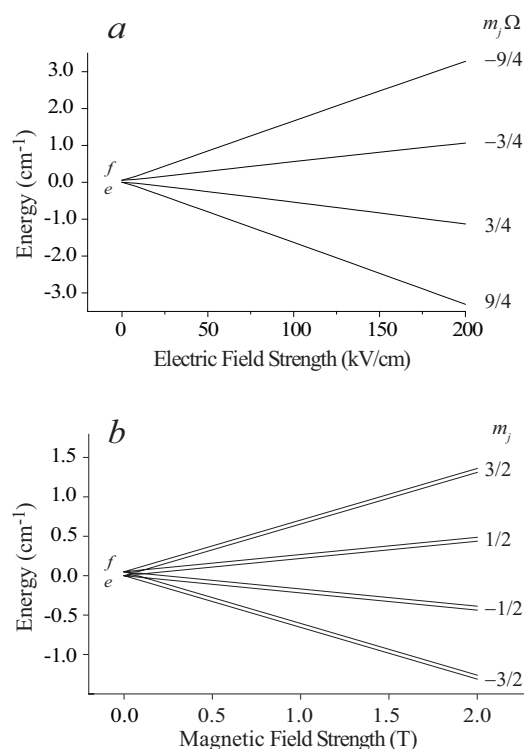
Fig. 4 Stark (panel a) and Zeeman (panel b) energy level diagrams of the $j = 3/2$ rotational ground state of OH ($X\,^2\Pi_{3/2}$). In zero field, the $j = 3/2$ rotational state is split into two Λ-doublet components of opposite parity, that are labeled e and f.

'high-field-seeking', respectively. The resulting Stark energy curves are shown in Fig. 4. It can be shown that the product $m_j\Omega$ is always negative for the upper Λ-doublet of f parity, whereas $m_j\Omega > 0$ for the lower component of e-parity.

We now turn our attention to the Zeeman effect. The magnetic dipole moment of a molecule consists mainly of contributions from both the orbital $\vec{L}$ and spin $\vec{S}$ angular momenta of the electrons. The Hamiltonian describing the interaction of a molecule and a magnetic field $\vec{B}$ is then given by

$$H_{\text{Zeeman}} = \frac{\mu_B}{\hbar}\vec{L}\cdot\vec{B} + \frac{2\mu_B}{\hbar}\vec{S}\cdot\vec{B}, \qquad (4)$$

where μ_B is the Bohr magneton with value $9.274 \cdot 10^{24}$ J/T. A similar vector diagram as presented in Fig. 3 can now be used to evaluate the Zeeman energies. For molecules in a $^2\Pi$ electronic state such as OH, the Zeeman energies are given by

$$U_{\text{Zeeman}} = \mu_B B \frac{m_j\Omega(\Lambda + 2\Sigma)}{j(j+1)}. \qquad (5)$$

The resulting Zeeman energy curves for OH ($X\,^2\Pi_{3/2}$) in the $j = 3/2$ rotational ground state are shown in Fig. 4. It is noted that unlike the Stark effect, the Zeeman effect does *not* mix the

two Λ-doublet states of opposite parity[10]. Consequently, each Λ-doublet components splits into four Zeeman levels, according to the possible values for m_j.

4 Controlling the internal quantum states of molecules

The change of internal quantum state upon a collision is one of the key processes underlying the exchange of energy between molecules. In bulk systems, such inelastic scattering events are responsible for the thermalization of state populations following after a chemical reaction. One of the most important goals experimentally is the measurement of state-to-state inelastic scattering cross sections at the full quantum state-selected level. For this, molecules ideally all reside in a single quantum state before the collision, and the population distribution over all quantum states after the collison is measured. In most cases, however, the quantum state purity that is reached in molecular beam expansions is not sufficient to measure pure state-to-state cross sections, and additional methods are needed to further purify the beam. In this section, we will discuss the methods that have been developed to produce molecular beams with almost perfect state purity.

4.1 State selection using multipole focusers

A powerful method for selecting the rotational quantum state of a symmetric top-like molecule possessing a permanent dipole moment is to use a multipole focuser[13]. The quadrupole and hexapole state selectors comprise four or six closely spaced, alternately charged rods, as schematically shown in Figure 5. An inhomogeneous electric field is generated between the rods, which is zero along the central axis of the selector and rises linearly or quadratically with radial separation from the centre, for a quadrupole and hexapole arrangement, respectively. The trajectory of a molecule through the state selector depends on its effective dipole moment and velocity on entering the system. The effective dipole moment in turn depends on the rotational state of the molecule. Based on the Stark effect (see section 3), molecules in high field seeking states are deflected towards the poles of the selector, and are ejected from the instrument. Conversely, molecules in low field seeking states are focused towards the central axis of the state selector.

The force $\vec{F}$ experienced by the molecules inside the state selector depends on the gradient of the Stark interaction energy. Consequently, for molecules with a predominantly quadratic and linear Stark shift, harmonic restoring forces $\vec{F} \sim -\vec{r}$ are obtained using the quadrupole and hexapole geometry, respectively. Molecules will follow sinusoidal trajectories inside the state selector, shown schematically in Figure 5. The ideal state-selector therefore acts as a perfect thin
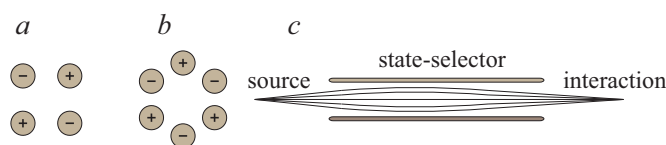
Fig. 5 Electrode arrangements used to create a quadrupole (*a*) or hexapole (*b*) field. Voltages with alternating polarity are applied to neighboring electrodes. Schematic representation of the focusing of molecules from the source into the interaction region (*c*).

lens, imaging the molecular packet from the source to the interaction region. The exact focusing properties depend on the shape of the Stark curve, the details of the field geometry, and the length of the state selector. More details can be found in Ref.[10].

The hexapole state selector is probably the most commonly employed as this provides good molecular focusing, without the excessive complexity that might be required with a higher multipole devices. Early applications of hexapole state selectors were to the study of the dynamics of alkali metal reactions with a range of symmetric top molecules. Many of these experiments also employed a static electric field after the hexapole to orient the molecule along a particular axis in the laboratory frame, as will be discussed in Section 5. Previous reviews of this work can be found, for example, in Ref.[7].

Since the 90's, there has been considerable interest in using hexapole state selection techniques to prepare open shell radicals, such as OH and NO, in well-defined quantum states prior to the collision. Both OH (*X*) and NO (*X*) have $^2\Pi_\Omega$ ground electronic states. Interest in these systems arises because collisions with the rare gases take place on two coupled (A′ and A″) potential energy surfaces, allowing a microscopic examination of the effects of the break down in the Born-Oppenheimer approximation. For many years, the scattering of OH or NO with rare gas atoms has been used as a prototype for the study of inelastic scattering of open shell molecules, and work up to 2010 has been reviewed recently[15].

As we have seen, within a given spin-orbit manifold of OH (*X*) and NO (*X*), each rotation state is split into two closely separated Λ-doublet levels, usually labelled *e* and *f*, which define the total parity of the diatomic. For low rotational states, the Λ-doublet splitting in OH (*X*) and NO (*X*) is much less than $1\,\mathrm{cm}^{-1}$, and under normal molecular beam expansion conditions both Λ-doublet levels are present in the beam with near-equal populations. Early studies of the inelastic scattering of NO (*X*), for example, were therefore performed with a near-equal mixture of the two initially populated Λ-doublet levels. However, the two Λ-doublet (parity) levels behave differently in the hexapole state selector, with only the low-field seeking upper Λ-doublet component of *f* parity being
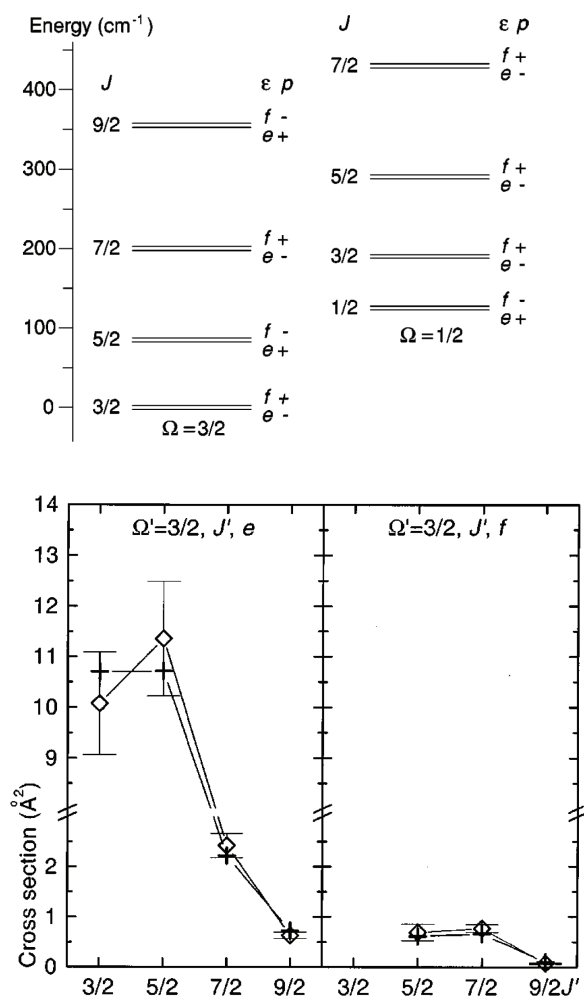
Fig. 6 Upper panel: Rotational energy level diagram of the OH ($X\,^2\Pi$) radical. The Λ-doublet splitting of each rotational level is greatly exaggerated for visual clarity. In collision experiments, the OH radicals can be prepared in the ($X\,^2\Pi, j = 3/2, f$) level by passing a beam of OH radicals through a hexapole state selector. Lower panel: State-to-state integral inelastic scattering cross sections for rotational excitation of OH ($X\,^2\Pi, j = 3/2, f$) into specific final rotational and Λ-doublet levels in collisions with Ar at a collision energy of 746 cm^{-1}. Reprinted with permission from Ref.[14]. Copyright 2000, AIP Publishing LLC.

focussed through the hexapole into the interaction region. The use of a hexapole state selector thus allows the preparation of these radicals in a specific Λ-doublet level, as well as in well-defined spin-orbit and rotational states.

The selection of a single Λ-doublet component prior to the collision has allowed for the study of inelastic scattering processes at the full state-to-state level. Perhaps one of the most striking results of these studies is the discovery of propensity rules for inelastic energy transfer. For excitation to a given final rotational and spin-orbit state, preferred excitation to one of the two Λ-doublet components of the final state can occur. This is illustrated for inelastic collisions between OH ($X\,^2\Pi_{3/2}, j = 3/2, f$) radicals and Ar atoms in the lower panel of Figure 6, that were obatained by ter Meulen and coworkers[14]. For spin-orbit conserving transitions, a strong preference for excitation into final states of e parity is observed, in close agreement with the predictions that follow from *ab initio* calculations. These propensities originate from the different expansion terms in the interaction potential that interfere either constructively or destructively for excitation into the e and f component of the final state, respectively. These propensity rules for rotational transitions are believed to play an important role in the formation of interstellar OH masers.

Recently, a relatively new class of this type of experiment emerged. In these experiments, hexapole state selection of the reagent molecules is coupled with product detection *via* resonantly enhanced multi photon ionization (REMPI) and velocity map ion imaging. These experiments allow fully quantum state-resolved differential cross sections to be determined. Results obtained by Eyles *et al.* for the inelastic scattering on NO (X) by Ar, shown in Fig. 7, provide an illustrative example of this kind of measurement[16]. These show differential cross sections (DCSs) obtained for a selection of final rotational states, generated subsequent to collisions of NO ($X\,^2\Pi_{1/2}$) in the $v = 0, j = 0.5, f$ with Ar[16]. The DCSs are colour coded according to whether or not the total NO parity is conserved (red continuous lines) or changes (green dashed lines) on collision. There are several features of note in the DCSs. Certain parity pairs of transitions separated by one in Δj are found to display similar DCSs (see, for example, the parity conserving [red] transitions for $j' = 7.5$ and $j' = 8.5$). This behaviour had been found previously in collisions of NO (X) + He, and arises from the fact that these neighbouring transitions of a given parity changing type are coupled by the same features (or expansion terms) in the interaction potential[17].

Another interesting observation concerning the DCSs shown in Fig. 7 is that those for parity conserving transitions (red lines) possess a multiple peaked structure, while those for parity changing collisions (green lines) show only a single peak. The structure was shown to arise from quantum mechanical interference, coupled with the near homonuclear nature of the NO (X) radical. The DCSs could be rationalised
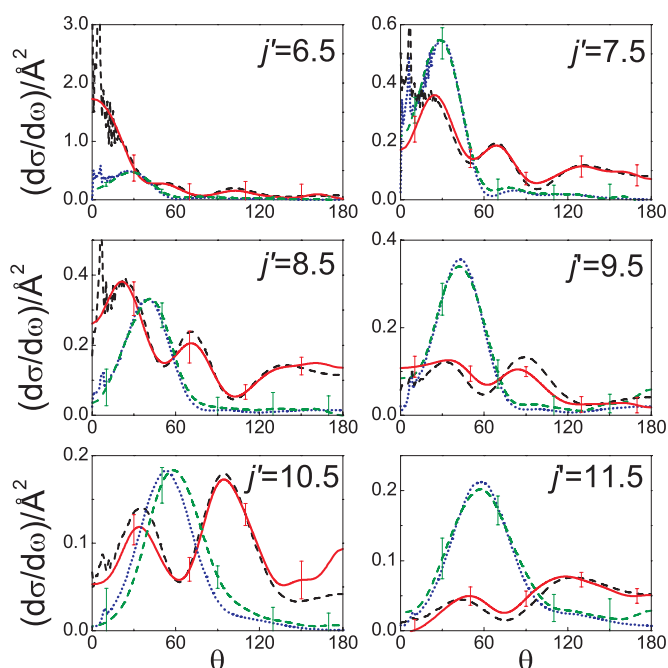
Fig. 7 Comparison of the DCSs for NO ($X^2\Pi_{1/2}$, $v=0$, $j=0.5$, f) + Ar inelastic collisions from experiment (red continuous lines - total parity conserving; green dashed lines - parity changing transitions) and CC QM theory (black dashed lines - parity conserving; blue dotted lines - parity changing transitions) at a collision energy of $530\,\mathrm{cm}^{-1}$. The initial state has negative total parity, $p = -1$, and the final states have parity $p = \varepsilon(-1)^{j'-1/2}$, such that total parity conserving transitions (in red) are those with $\Delta j = j' - j = $ even, f levels, and with $\Delta j = $ odd, e levels. Reprinted by permission from Macmillan Publishers Ltd: Nature Chemistry (Ref. [16]), copyright (2011).

qualitatively in terms of a simple four-path interference model, in which parity conserving transitions are primarily sensitive to interferences between scattering from the end and the sides of the molecule, whilst parity changing collisions are more sensitive to interference between scattering paths involving the two (only slightly different) ends of the molecule [16].

Fully quantum state resolved measurements of the DCSs obtained using hexapole state focusing methods have also been performed on scattering of OH (X) with He and Ar, and ND$_3$ with He, by Parker and coworkers [18]. The OH (X) system is a particularly challenging system experimentally because, unlike NO (X), OH (X) is highly reactive and must be generated *in situ* in the molecule beam expansion. In addition, REMPI detection of OH is notoriously difficult. In the case of ND$_3$, hexapole state focusing allows selection of molecules in those specific states which are antisymmetric with respect to inversion *via* the ND$_3$ umbrella mode. As with the parity selection in NO (X) and OH (X), the DCSs were found to be highly sensitive to whether or not the inversion symmetry of

ND$_3$ is conserved during collision. Both sets of experiments for OH (X) and ND$_3$ showed good qualitative agreement with quantum mechanical scattering calculations.

Magnetic state selectors have been developed as well, and are either composed of current carrying wires or consist of an assembly of permanent magnets. The influence of magnetic state selectors on the field of molecular collisions has been considerably smaller compared to electric state selectors, however. Perhaps the properties of the Zeeman effect itself (see section 3) is the reason for this historical asymmetry. For instance, selection of a single Λ-doublet component of diatomics such as OH (X) or NO (X) using magnetic fields alone is not possible – both Λ-doublet components possess low and high field seeking sublevels. For other species, such as O$_2$, NH and metastable atoms, magnetic quadrupole or hexapole focusers can be used to state-select a molecular beam. Recently, magnetic hexapoles have been developed that were used in a series of experiments to study steric effects in atom-molecule reactions [19] (see section 5).

4.2 State selection using deflectors

The purification of beams using hexapole or quadrupole focusing works well for relatively small molecules that have a rather simple energy level structure. For large polyatomic molecules, however, state-selection using multipole fields is usually not possible, as these large molecules typically possess a high density of internal quantum states that are all high-field seeking. Unfortunately, no electrode geometry can be made that creates an electric field maximum at the molecular beam axis. Instead, electric deflection fields can be used to spatially separate molecules in different internal quantum states. A deflector typically consists of two electrodes with a shape that is designed to generate a strong force on the molecules in one direction, while the force in the perpendicular direction is zero (see inset to Figure 8). Molecules in states that possess a different dipole moment will follow different trajectories inside the deflector, which can be exploited to prepare pure samples of molecules in selected quantum states [10].

Chang *et al.* developed an experimental approach, based on spatial separation of conformers using electrostatic deflection, that allows for the measurement of conformer-specific reaction rates [20], see Figure 8. Conformers are different versions of a particular molecule, but with different geometric structures that interconvert with low thermal barriers through rotations about covalent bonds. These conformers can display different reactivity in bimolecular reactions. However, it is very challenging to select a single conformer in a molecular beam, and to study the conformer-selective reactivity in a collision experiment. Chang *et al.* used a molecular beam of 3-aminophenol (AP), and passed it through a 15-cm long electric deflector. AP exhibits two distinct molecular conformations,

cis and trans, that differ in the relative orientation of the OH bond with respect to the NH_2 group. Both conformers have significantly different electric dipole moments of 0.77 D and 2.33 D for the trans and cis species, respectively, resulting in a spatial separation of the two conformers. The separated conformers react with a target of Coulomb-crystallized Ca^+ ions in a trap, that can be mechanically moved along the y-axis. Rate constants for the reaction of Ca^+ with 3-aminophenol were determined from the observed decrease of the number of Ca^+ ions in the crystals. A two-fold larger rate constant was found for the cis compared with the trans conformer. This result could be explained by the conformer-specific differences in the long-range ion-molecule interaction potentials, arising from differences is dipole moment of the two conformers.
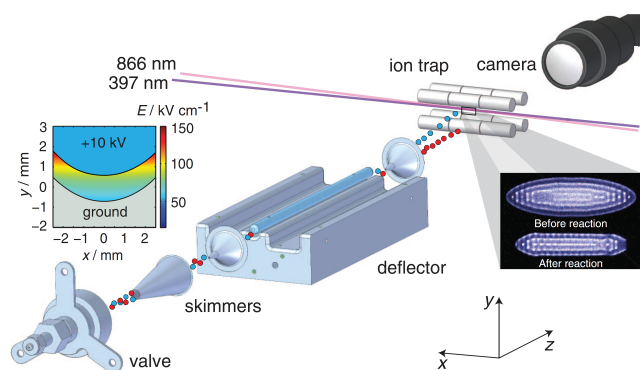
Fig. 8 Experimental set-up used by Chang *et al.* to study conformer-selective reaction rates for reactions between Ca^+ ions and 3-aminophenol. The cis and trans conformers are spatially separated by passing the beam of 3-aminophenol through an electric deflector. From Ref.[20]. Reprinted with permission from AAAS.

5   Controlling the orientation of molecules

A central concept in chemistry is that of the steric effect. The relative arrangement of atoms or groups of atoms within a molecule is a fundamental issue in chemistry, and defines the related field of stereochemistry. The ability to control the relative orientation of isolated molecules in the laboratory provides a unique opportunity to study steric effects at a microscopic level.

We start with a few definitions. When considering the polarization of molecules, it is helpful to distinguish molecular orientation and alignment. Molecular orientation is present when a particular end of a molecule points in a specific direction, while molecular alignment refers to polarization of a molecule along a particular axis. Thus, for an aligned molecule, the two ends of the molecule will point with equal probability in either direction along the alignment axis. In the context of

polarization effects, it is also important to distinguish molecular (bond) axis versus angular momentum orientation and alignment. These two quantities are closely related, because a molecule with a well-defined angular momentum polarization will also possess a characteristic molecular (bond) axis distribution. Furthermore, a molecule with a well-defined molecular axis orientation can be described by a coherent superposition of angular momentum quantum states. When studying inelastic and reactive scattering it is often more convenient or appropriate to consider molecular axis orientation in the reactants, but rotational angular momentum polarization of the reaction products. Most of the discussion below will therefore focus on the polarization of molecular axes of reactant molecules.

Orientation of molecules can be achieved by coupling the hexapole state selector, described in Section 4.1, with a static electric field, which is applied to the molecules just as they leave the hexapole state selector and enter the interaction region (see Fig. 9). The static field serves to adiabatically reorient the molecules exiting the hexapole to a well-defined axis in the laboratory, given by the direction of the electric field[7]. By changing the direction of the electric field with respect to the relative velocity of the collision system, it is possible to investigate the dependence of the scattering cross sections on 'heads versus tails' orientation of the molecule with respect to the collision partner.

The technique is applicable to those symmetric top-like molecules systems which are amenable to hexapole state selection. This includes simple open-shell diatomic radicals such as OH (X) and NO (X), which are usually preselected in their lowest rotational states. It is important to realize, however, that one must be careful with this 'classical picture' of orientation of the bond axis. Referring back to section 3, the effect of the electric field is such that the expectation value of $\cos\theta$, where θ is the angle between the dipole moment of the molecule and the direction of the orientation field, has a certain value. For the species OH (X) and NO (X), for instance, the static electric field produces a coherent superposition of Λ-doublet levels, such that

$$\langle\cos\theta\rangle = m_j\Omega/j(j+1). \tag{6}$$

For the rotational ground states of OH (X) and NO (X) this results in $\langle\cos\theta\rangle = 0.60$ and $\langle\cos\theta\rangle = 0.33$, respectively.

There have been several recent applications of this technique to the study of the orientation dependence of the integral cross section, both in inelastic and reactive scattering. The first investigations of inelastic scattering were performed on the NO (X) + Ar system by Stolte and coworkers in the mid-to-late 90's[23], with subsequent experiments reported by ter Meulen and coworkers for scattering of OH (X) with Ar[22], and CO and N_2. The experiments on OH (X) + Ar have additional been extended to investigate reorientation collisions,
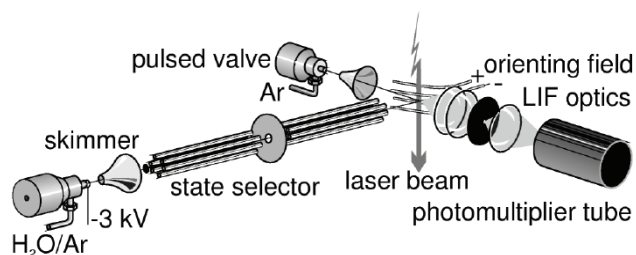
Fig. 9 A schematic diagram of the apparatus used to study the dependence of the cross section for inelastic scattering of OH (X) by Ar with OH (X) bond axis orientation[21]. In these experiments, the scattered OH (X) radicals were detected using laser induced fluorescence (LIF), which was observed close to the interaction region using a photomultiplier tube. Reprinted with permission from Ref.[22]. Copyright 2000, AIP Publishing LLC.

Fig. 10 Experimental (filled circles and triangle connected by solid and dashed lines respectively) and theoretical (open circles and triangles) results for the steric asymmetry of spin-orbit state conserving collisions of Ar and NO (X). The initial state of the NO ($X\,^2\Pi_{1/2}$) is $v = 0$, $j = 0.5$. Note that the steric asymmetry ratio appears to depend strongly on the j' value and only weakly on the parity of the final state. The state with $j' = 15.5$ is the highest energetically allowed. Reprinted from Chemical Physics Letters, Ref.[23], Copyright (1999), with permission from Elsevier.

in which cross sections for m_j changing collisions have been quantified[21]. Most of these experiments were performed using laser induced fluorescence detection of the inelastically scattered products, and a schematic diagram of the apparatus used for the OH (X) studies is shown in Fig. 9.

Results in this field are usually reported in terms of the steric asymmetry, which is the normalized difference in the cross section for inelastic scattering off the two ends of the oriented diatomic molecule. For OH (X) + Ar collisions, for instance, rotational excitation was found to be more likely if the Ar atom strikes the OH radical at the H-end rather than at the more massive O-end, in full agreement with what one would expect using classical arguments[22]. Good agreement has generally been found between experiment and quantum scattering calculations, and the results can be interpreted in terms of the anisotropy of the potential energy surfaces involved. For most systems, however, classical arguments fail to account for the observed steric effects and a full quantitative understanding of steric asymmetry factors requires a quantum dynamical description. In this respect, the scattering of NO(X) with Ar provides a famous and particularly illustrative example[23]. As shown in Fig. 10, for NO ($X\,^2\Pi_{1/2}$) molecules initially in the $v = 0$, $j = 0.5$ level, strong oscillations in the steric asymmetry are observed as a function of the final rotational state, j'. These have been shown to be quantum mechanical in origin, reflecting interference between scattering off the two ends of the NO (X) molecule[24].

In a set of beautiful experiments, Kasai and coworkers used similar techniques to study reactive scattering between oriented atoms and molecules. For instance, the orientation dependence of Br atom formation was measured for reactions between hexapole state-selected and oriented OH radicals with HBr molecules[25]. It was found that O-end attack is most favored for this reaction, that H-end attack also shows a

pronounced reactivity, while reactivity at side-ways attack is small. The results suggested the existence of two different reaction pathways. Reaction by O-end attack is followed by a direct abstraction of the H-atom from the HBr molecule. The mechanism for H-end attack may have H-atom migration from HBr to form the water molecule.

In an important extension of this class of experiments, Kasai and coworkers have measured the steric effect for dissociative energy transfer in the reaction Ar ($^3P_2$) + CF_3H[19], in which both reactants were oriented. The progress of the reaction was monitored by observing the chemiluminescence from the CF_3 products. A hexapole electric field was used to select the state of CF_3H, which was subsequently oriented in a static electric field. The total electronic angular momentum of the Ar ($^3P_2$) was selected in the $m_j = 2$ sub-level using a magnetic hexapole state selector, and the atom was subsequently oriented in the interaction region using a magnetic field. The experiments revealed significant variations in reactivity depending on the mutual configuration of the molecular and atomic orientation.

Much of the pioneering work on the use of hexapole state selection coupled with static orientation fields dates back to the work of Bernstein and coworkers in the 60's and 70's, in which in also information on the angular distribution of the products was obtained. In spite of these early pioneering experiments, there remains to this day rather few exam-

ples of measurements of the orientation dependence of differential cross sections, and, to our knowledge, none of these have achieved full quantum-state resolution in both reactant and product channels.

The molecular axis of molecules with a permanent dipole moment can also be oriented using a 'brute force' method, in which the molecule is placed in a strong homogeneous electric field[26]. When the field is sufficiently strong, and the molecules sufficiently rotationally cold, a coherent superposition of rotational states can be generated, and the molecules experience a restraining force which leads to pendular-type motion in the electric field. The degree of orientation achievable depends on the strength of the dipole moment, the applied field, and the rotational energy of the molecule. The more rotational energy the molecule possesses, the harder it is to achieve significant bond-axis orientation in an electric field of reasonable strength, so the brute force orientation method is usually performed on molecules cooled in supersonic molecular beams. The orientation technique has been used by Loesch and coworkers to measure the differential cross sections for oriented molecules[27].

The focus of the present review has been the orientation and alignment of molecules using external electric or magnetic fields. However, it is important to note that bond-axis alignment of molecules can be achieved using optical methods, using photon absorption or Raman pumping techniques[28]. Indeed, the distinction between optical and external field methods can become blurred, particularly when using the strong electric fields present in intense femtosecond laser pulses[29]. For example, non-resonant nanosecond laser pulses can be used to adiabatically three-dimensionally align molecules in space, with the degree of alignment controlled by the strength of the applied laser field. Impulsive, non-adiabatic alignment can also be achieved using short femtosecond laser pulses[29]. This can be thought of as a non-resonant stimulated Raman process, which leads to the coherent superposition of rotational states required for molecular axis alignment. So far these types of alignment experiments have only been performed in connection with studies of molecular photon-induced dynamical studies, but it is likely that some of these methods will be employed in collisional studies in due course.

While the above discussion has focussed on the orientation and alignment of the molecular axis, it should also be noted that polarized light can be used to orient and align the angular momentum, $\vec{j}$, of an atom or molecule. For example, there has been much recent work on the collisions of rotationally oriented and aligned diatomic molecules (see recent reviews, Refs. [30,31]). Polarization spectroscopy[30] and Zeeman quantum beat spectroscopy[31] have recently been the favoured methods used to interrogate the collisional loss of angular momentum orientation and alignment. In the present context, the Zeeman quantum beat technique illustrates how an external magnetic

field can be used to pre-orient rotational and electronic angular momentum for molecular collision studies, something which has recently also been graphically illustrated for polarized $O(^1D_2)$ atoms[32]. In these experiments, the atoms were generated by photolysis of O_2 at 157 nm, and orbital polarization of the atomic fragments monitored at various pump-probe delay times using velocity map ion imaging. In the presence of a magnetic field, the atomic polarization generated in the photolysis step was observed to precess around the field direction in a similar way to that observed in magnetic resonance. This control could be used in collisional studies of the effect of electronic orbital angular momentum polarization on chemical reactivity.

6   Controlling the velocity of molecules

Arguably one of the most important parameters in a collision experiment is the collision energy, i.e., the relative velocity with which the particles undergo a scattering event. Control over the collision energy has been a difficult experimental task, however. The speed of a molecular beam is set by the temperature of the nozzle and the gas that is expanded, and until recently, little can be done to precisely control the velocity of molecules in the beam. Mechanical velocity selectors can be used to select molecules with a narrow velocity distribution out of the beam, but the particle densities and velocities that can be reached are set by the original velocity distribution of the beam. With fixed beam speeds, the collision energy can be tuned by mechanically varying the crossing angle of the intersecting beams, allowing variation of the collision energy while maintaining high enough particle densities for scattering.

Exquisite control over the velocity of molecules in a molecular beam has become possible by the development of beam deceleration methods. In these devices, the interaction of molecules with electric or magnetic fields is used to change their longitudinal velocity, i.e., to decelerate or accelerate them. For this, time-varying field gradients along the propagation direction of the molecular beam are required, that are arranged such that molecules are accelerated or decelerated similar to the manipulation of charged particles in a linear accelerator (LINAC). This was first demonstrated in 1998 by Meijer and coworkers who slowed down a molecular beam of metastable CO molecules in a so-called Stark decelerator[33]. The deceleration (or acceleration) process can be seen as slicing a packet of molecules with a narrow velocity distribution out of the densest part of the molecular beam pulse. This packet can then be decelerated or accelerated to any velocity, maintaining the narrow velocity distribution and the particle density in the packet. As the deceleration process is quantum-state specific, the bunches of slow molecules that emerge from the decelerator are extremely pure, and quantum state purities

of better than 99.9 % can be reached. The operation principles of Stark decelerators and related devices have been thoroughly described in Ref[10].

These monochromatic and pure beams with a tunable velocity are excellent starting points for molecular beam scattering experiments. The first scattering experiment using a beam of Stark-decelerated molecules was performed in 2006 by Gilijamse *et al.*. A packet of OH radicals was tuned in velocity between 33 m/s to 700 m/s using the Stark decelerator, and scattered with a conventional beam of Xe atoms in a crossed molecular beam geometry[34]. The state-to-state integral scattering cross sections for excitation out of the upper Λ-doublet component of the $X,^2\Pi_{3/2}, j = 3/2, f$ rotational ground-state of the OH radical were measured. The total center-of-mass collision energy was varied from 50 cm^{-1} to 400 cm^{-1}, and the threshold behavior for inelastic scattering into the first excited rotational levels of the OH radical were accurately determined.

Scharfenberg *et al.* constructed an improved version of the Stark decelerator that is optimized for crossed beam scattering experiments. This 2.6-meter-long Stark decelerator was used to study inelastic scattering of OH radicals with Ar atoms as a function of the collision energy. Scharfenberg *et al.* showed that this decelerator enabled state-to-state scattering experiments to be performed with a sensitivity that can compete with the sensitivity that is obtained in conventional crossed beam scattering experiments[35]. In Figure 11 the measured relative state-to-state inelastic cross sections are shown for OH-Ar collisions as a function of the center-of-mass collision energy. Excitation from the $X,^2\Pi_{3/2}, j = 3/2, f$ initial state into 13 final states was measured. The largest cross section is observed for scattering into the $(X^2\Pi_{3/2}, j = 3/2, e)$ state. This Λ-doublet changing collision is the only exo-energetic channel, and the relative cross section for this channel therefore approaches 100 % at low collision energies. The other channels show a clear threshold behavior. The solid curves that are shown in the figure are the relative inelastic scattering cross sections that result from quantum scattering calculations, which are seen to be in excellent agreement with the experiment.

The approach was taken a significant step further by Kirste *et al.*, who replaced the conventional beam to produce the atomic collision partner with a beam of hexapole state-selected NO radicals[36], as illustrated in Figure 12. Stark-decelerated OH $X,^2\Pi_{3/2}, j = 3/2, f$ radicals were scattered with the hexapole state-selected NO $X,^2\Pi_{1/2}, j = 1/2, f$ radicals, facilitating the first study of rotational energy transfer between two open-shell molecules that are both prepared in a single quantum state. Major obstacles exist that had prevented earlier studies of state-to-state bimolecular scattering. The main challenge is the need for reagent beams with sufficient quantum-state purity at the densities necessary to observe pop-
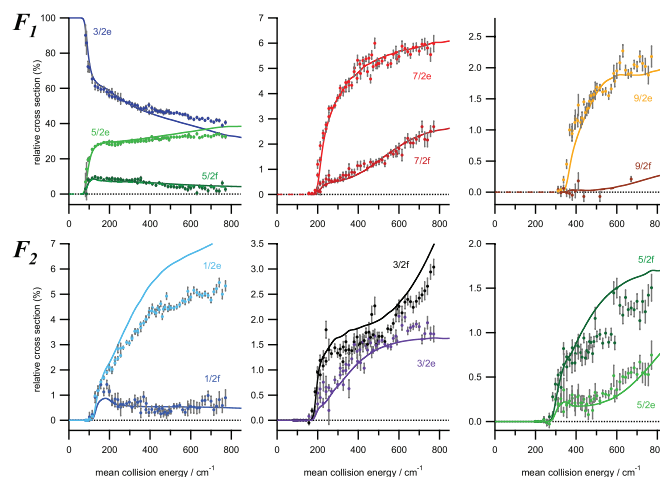
Fig. 11 Relative inelastic cross sections for scattering of OH $(X^2\Pi_{3/2}, j = 3/2, f)$ radicals with Ar atoms as a function of the center-of-mass collision energy. The relative state-to-state inelastic scattering cross sections for collisions populating rotational levels in the $F_1(X^2\Pi_{3/2})$ and the $F_2(X^2\Pi_{1/2})$ spin-orbit manifolds are shown in the top and bottom row, respectively. The relative cross sections that result from quantum close-coupled calculations based on recent high-quality *ab initio* OH-Ar PES's are given by the solid curves. Reproduced from Ref.[35] with permission from the PCCP Owner Societies.

ulation transfer in one, or both, reagent beam(s). Kirste *et al.* overcame these obstacles exploiting the high state-purity of the Stark-decelerated packets of OH radicals. The peak densities of the reagent OH and NO packets were determined to be $(2 \pm 0.8) \times 10^8$ cm^{-3} and $(9 \pm 3) \times 10^{10}$ cm^{-3}, respectively. Only a fraction of $10^{-4} - 10^{-6}$ of the OH radicals were inelastically scattered, but the state-purity of 99.99 % of the reagent OH packet allowed nevertheless for the state-selective detection of the scattering products. Rotationally and spin-orbit inelastic scattering cross sections were measured for collision energies between 70 and 300 cm^1, as shown in Figure 12. The extremely well-defined spatial distributions of the OH and NO packets also allowed for the unique opportunity to experimentally determine the scattering cross sections on an absolute scale.

In contrast to the scattering of OH or NO with rare gas atoms, *ab initio* calculations of multiple anisotropic PESs with their nonadiabatic couplings for OH-NO are beyond the capabilities of current theoretical methods. Therefore, the inelastic scattering process was modeled assuming that the measured scattering channels are governed by the long-range electrostatic interactions, which can be calculated accurately by *ab initio* methods. The resulting cross sections showed remarkable agreement with the experimentally determined cross sections, revealing the crucial role of electrostatic forces in these
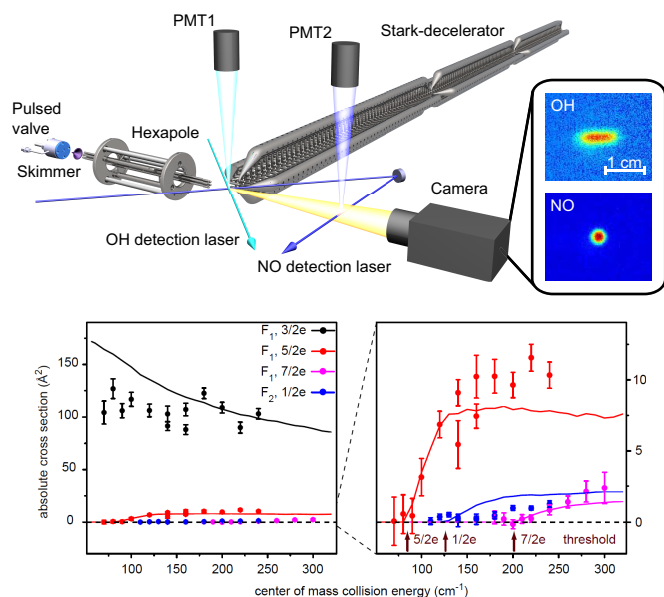
Fig. 12 Top panel: Arrangement used by Kirste *et al.* to study the inelastic scattering between Stark-decelerated OH $X,^2\Pi_{3/2}, j = 3/2, f$ radicals and hexapole state-selected NO $X,^2\Pi_{1/2}, j = 1/2, f$ radicals. Lower panel: Experimentally determined absolute state-to-state inelastic scattering cross sections (data points), together with the cross sections that result from a theoretical model of the scattering process (solid curves). From Ref. [36]. Reprinted with permission from AAAS.

complex molecular collision processes.

Recently, Von Zastrow *et al* combined the Stark deceleration technique with the velocity map imaging technique in a crossed beam experiment[37]. A packet of NO $X,^2\Pi_{1/2}, j = 1/2, f$ radicals with a fixed velocity of 370 m/s and a velocity spread of 2.4 m/s was produced by passing a beam of NO through a Stark decelerator, see Figure 13. State-to-state differential cross sections for rotationally inelastic collisions between the NO radicals and He, Ne and Ar were studied at a fixed collision energy of 630 cm^{-1}, 485 cm^{-1} and 450 cm^{-1}, respectively. The monochromatic velocity distribution of the NO beam produced scattering images with unprecedented sharpness and angular resolution. This was exploited to fully resolve quantum diffraction oscillations in the DCSs, as is shown in Figure 13. Diffraction oscillations originate from quantum interference between different trajectories of the colliding molecules on the PES leading to the same final deflection angle. The resulting rapid oscillations are among the most detailed structures that can occur in any DCS.

Recently, Zeeman decelerators – the magnetic analogs of the Stark decelerator – have been developed as well. Using a series of coils through which time-varying currents are passed, the successful deceleration of various atomic species, O_2
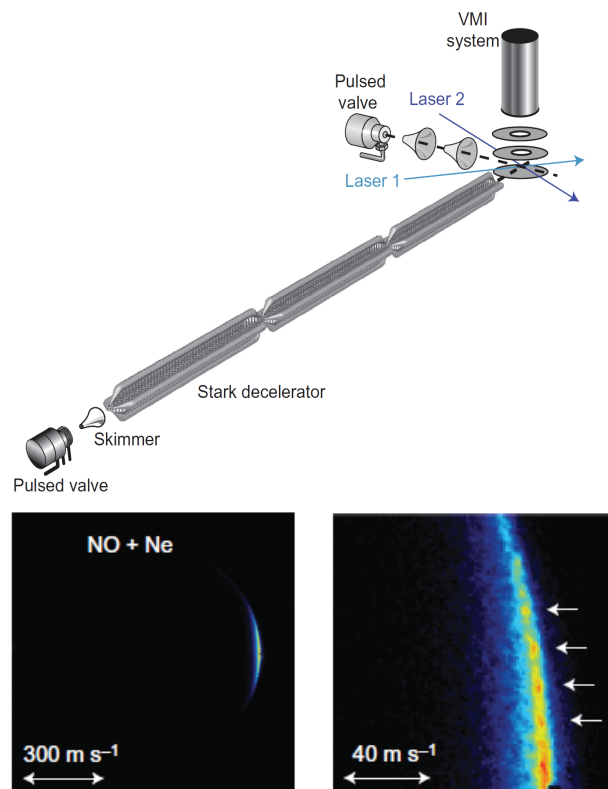
Fig. 13 Top panel: Arrangement used by von Zastrow *et al.* to measure differential cross sections for inelastic scattering of velocity controlled NO $X,^2\Pi_{1/2}, j = 1/2, f$ radicals with rare gas atoms. A Stark decelerator is used to prepare the NO radicals prior to the collision, and a velocity map imaging detector is used to detect the scattered NO radicals. Lower panel: Experimental ion images revealing quantum diffraction oscillations for NO-Ne collisions. Reprinted by permission from Macmillan Publishers Ltd: Nature Chemistry (Ref. [37]), copyright (2014).

molecules, as well as the CH_3 radical has already been demonstrated[38]. The Zeeman deceleration technique increases the chemical diversity of particles that can be velocity controlled, and holds great promise for future collision experiments.

7 Cold collisions

In the last few years, there has been a growing interest in the study of molecular collisions at low collision energies[39]. Cold collisions are governed by rich quantum phenomena foreign to high-energy collisions, such as tunnelling and scattering resonances. Scattering resonances appear when the collision energy is resonant with the internal energy of a (quasi-) bound state of the collision complex, resulting in dramatic changes in the collision cross section. These scattering resonances are

extremely sensitive to the exact topology of the molecular interaction.

The experimental study of low-energy molecular collisions has proven very difficult, as access to this energy regime is difficult using molecular beams that typically travel at high speeds. The beam manipulation techniques discussed in the previous sections offer fascinating possibilities to reach the low collision energies, and the appropriate energy resolutions, for a large variety of systems. In recent years, several approaches have been followed to use electric and magnetic beam manipulation tools to study molecular scattering phenomena at ever lower collision energies. These are discussed in the next sections.

7.1 Low energy collisions using particle traps

Using Stark or Zeeman decelerators, packets of molecules can be slowed down to standstill, and stored in traps for times up to seconds. These trapped samples of molecules have a velocity distribution corresponding to temperatures in the mK range, and are excellent starting points for low energy collision experiments. Ye and coworkers developed a trap consisting of permanent magnets to confine OH radicals decelerated to a near standstill using a Stark decelerator[40]. Collisions with the OH radicals were studied by sending supersonic beams of He atoms or D_2 molecules through the trap[40]. Information on the total collision cross sections could be inferred from the beam-induced trap loss that occurs through elastic as well as inelastic collisions. The approach was later refined by combining it with the buffer gas cooling technique[41], as is illustrated in Figure 14. A continuous buffer gas cooled beam of state-selected ND_3 molecules was directed via a curved hexapole through a magnetically trapped sample of OH radicals, allowing interaction times of ~ 1 s. Only the slowest ND_3 molecules were transmitted through the curved guide, and the total cross section for collisional trap loss could be measured at a mean collision energy as low as 3.6 cm^{-1}. A polarizing electric field was applied to the magnetic trap, and first indications for the influence of an applied field on the cross sections were observed.

Similar approaches have been developed to study ion-molecule reactions at low collision energies. In 2008, Willitsch *et al.* combined a source of laser-cooled ions in a linear Paul trap with a curved electrostatic quadrupole guide to filter the low-velocity distribution from an effusive beam of polar molecules[42]. Reactive collisions between trapped Ca^+ ions and translationally cold CH_3F molecules were studied at temperatures ≥ 1 K by monitoring the decrease of the number of Ca^+ ions observed in the fluorescence images. The disappearance of individual ions could be observed as a function of the time of exposure to the flow of CH_3F, yielding directly the bi-molecular rate constant of the reaction. An extension
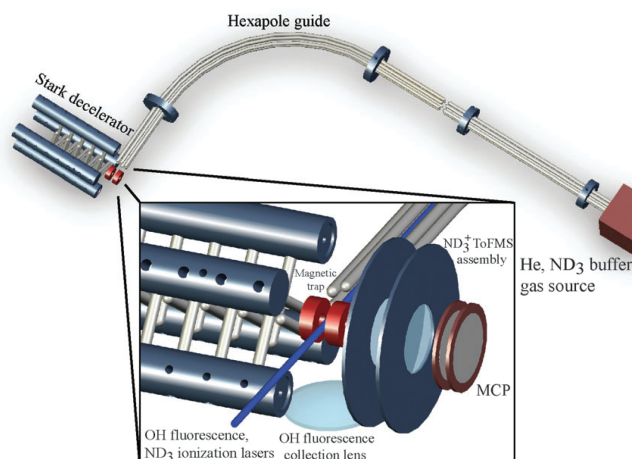
Fig. 14 Experimental set-up used by Sawyer *et al.* to study collisions between OH racicals and ND_3 molecules at collision energies down to 3.6 cm^{-1}. The OH radicals are decelerated to standstill using a Stark decelerator, and confined on a magnetic trap consisting of permanent magnets. A continuous beam of ND_3 molecules is directed through the trap by the curved electrostatic guide, transmitting selectively the slowest ND_3 molecules from the beam distribution. Reproduced from Ref.[41] with permission from the PCCP Owner Societies.

of the experimental approach for the study of low-temperature reactions with sympathetically cooled molecular ions (translational temperature T > 10 mK) was presented by Bell *et al.*, together with first results on the charge-transfer reaction between OCS^+ ions and velocity filtered ND_3 molecules[43].

Lower collision energies can be obtained if all particles that are involved in the collision are confined in a trap. Lewandowski and coworkers produced a sample of Stark-decelerated ND_3 molecules, and stored them in an electrostatic quadrupole trap. The trap containing the ND_3 molecules was then superimposed with a sample of magnetically trapped Rb atoms by mechanically moving the magnetic trap to the electrostatic trapping region[44]. Collisions between the ND_3 molecules and Rb atoms were studied at milliKelvin temperatures by monitoring the decay of the ND_3 density in the trap. The observed inelastic collision cross sections were larger than expected for field-free collisions. This increased collision rate was rationalized via quantum-mechanical scattering calculations on Rb-ND_3 collisions in the presence of an electric field.

Ye and coworkers produced a sample of Stark-decelerated OH radicals, and confined the OH radicals using magnetic fields. With electric fields superimposed to the trapping region, inelastic two-body collisions between the trapped OH radicals was observed. In combination with microwave fields that can drive transitions between the two Λ-doublet compo-

nents of the rotational ground state of OH, a pathway was found to selectively remove the hottest molecules from the trap. This enabled the first demonstration of forced evaporative cooling of a diatomic molecule[45].

Novel collision experiments have also been conducted between atoms and molecules that are co-trapped in a magnetic trap via buffer gas cooling[46]. Rather than by using electric or magnetic fields, in this approach atoms and molecules are cooled by collisions with cryogenically cooled He atoms. Magnetic fields are then used to confine the atoms and molecules in a trap, in which their scattering properties can be studied.

7.2   Low collision energies by merging molecular beams

In principle, low collision energies can also be obtained using molecular beams with high speeds, provided that the *relative* velocity between the two beams is low. This can, for instance, be obtained by using a small crossing angle between the two beams. This approach has recently been followed by Costes and coworkers, who developed an ingenious crossed beam apparatus with variable crossing angle, in which the lowest crossing angle that can be obtained amounts to 12.5°. For favorable systems such as $CO + H_2$ and $O_2 + H_2$, this allowed for the measurement of scattering resonances in state-to-state integral cross sections at energies down to a few cm^{-1}[47].

Henson *et al.* took this concept a step further, and obtained a zero degree crossing angle by merging two molecular beams[48]. Relative velocity, and thus the collision energy, approaches zero in a moving frame of reference when beams of equal velocities merge. The Zeeman effect was exploited to direct a beam of metastable He atoms through a curved magnetic quadrupole guide, see Figure 15. At the exit of the quadrupole, the beam of metastable He atoms merges with another supersonic beam of Ar atoms or H_2 molecules that has travelled in a straight line from a separate supersonic source. By varying the temperature of the beam sources, reactions rates for the Penning ionization of Ar and H_2 with metastable He was measured at collision energies from 350 K to 10 mK. By dispersing the velocity components of the molecular beam during their travel time in the guide, high collision energy resolutions were obtained. At energies below a few K, orbiting resonances were clearly observed, leading to sharp increases in the Penning ionization reaction rates.

The energies which the resonances are found are very sensitive to the exact details of the potential energy surface. By replacing the H_2 beam with beams of D_2 or HD, strong isotope effects in the Penning ionization reaction rates were observed[49]. These effects can be rationalized from the change in reduced mass of the collision pair, and the corresponding changes in centrifugal energy. These, in turn, have large effects on the energies of quasi-bound states of the collision

pair, resulting in different energies at which the scattering resonances occur.

Recently, Osterwalder and coworkers at EPFL Lausanne, Switzerland, developed a merged beam experiment in which *two* curved guides were employed[50]. A beam of metastable Ne atoms was passed though a curved magnetic guide, while a beam of ND_3 molecules was passed through a curved electric guide. Both beams were then merged downstream from the guides. Penning ionization reaction rates were measured at collision energies down to 100 mK.
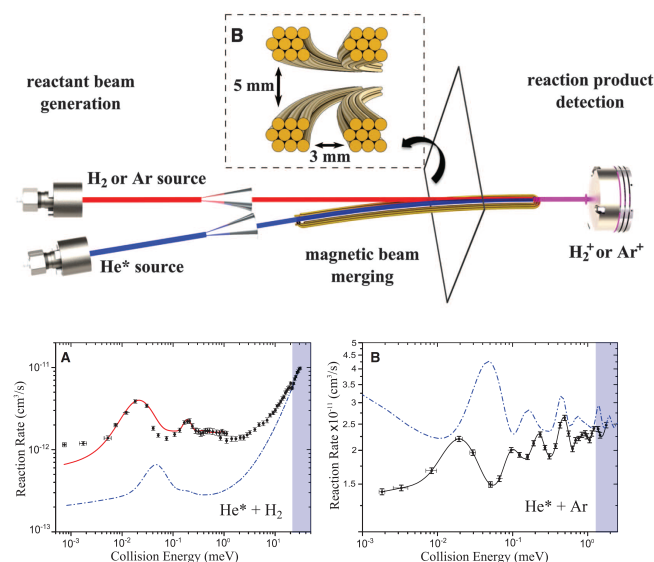
Fig. 15 Merged molecular beam set-up used by Henson *et al.* to obtain collision energies down to 10 mK. A beam of metastable He atoms is directed through a curved magnetic guide, and merged with another beam that travels in a straight line. From Ref.[48]. Reprinted with permission from AAAS.

8   Conclusions

With this Tutorial Review we hope to convey the activity and excitement in current research on molecular collisions made possible by recent technical advances in molecular beam control and nascent molecule detection methods. The premise is that knowledge on the isolated molecule scale underpins our understanding of all chemistry, which is certainly the case for many important fields such as astrochemistry and combustion. The beauty of research in molecular collisions is that all that is measured can also in principle be fully predicted at the *ab initio* level of quantum theory. Herein lies also a handicap in making rapid steps towards larger and more complex systems: theory is not yet capable of describing systems with more than ~ 6 atoms on an *ab initio* basis. Furthermore, the

transport of increasingly larger molecules into single collision gas phase conditions provides an experimental challenge; one with immediate applications, however, in mass and other types of spectrometry, as shown here in the case of conformer selection. Ultra-sensitive and ultra-selective methods developed in this gas-phase research field are finding new applications in studies of gas-surface interactions, in reacting molecules solvated, for example, in liquid helium droplets and, in general, in cluster research bridging the gap from gas to condensed phases.

As shown in this Review, an important development in the field is that increasingly difficult but relevant molecules such as the hydroxyl radical are being tackled, and this trend should continue in tandem with progress in laser preparation and detection schemes, involving also new sources of laser radiation tunable from the extreme-ultraviolet to far-infrared. Further down the road, it can be expected that full three-dimensional Newton spheres for reactive and inelastic scattering will be measured, revealing complete multi-dimensional vector correlations between pre- and post-collision properties. This is important not only for esthetic reasons but also because azimuthal symmetry is often broken in experiments using tamed molecular beams, in particular when combined with polarized light to probe polarization effects.

Over the last decades, devices have been developed to deflect, focus, orient, or decelerate molecules, and have found applications in collision experiments with ever increasing complexity. These new devices boosted the measurement resolution, aiding our efforts to unravel the quantum mechanical nature of molecular interactions. As is often the case in advances in technique, in the years to come they should provide more unexpected breakthroughs in the progress of understanding molecular change.

9 Acknowledgements

References

1 W. Gerlach and O. Stern, *Z. Phys.*, 1922, **9**, 349–352.

2 J. P. Gordon, H. J. Zeiger and C. H. Townes, *Phys. Rev.*, 1954, **95**, 282–284.

3 H. G. Bennewitz, W. Paul and C. Schlier, *Z. Phys.*, 1955, **141**, 6–15.

4 J. P. Toennies, *Discuss. Faraday Soc.*, 1962, **33**, 96.

5 H. Bennewitz, K. Kramer, W. Paul and J. Toennies, *Z. Phys.*, 1964, **177**, 84–110.

6 P. R. Brooks and E. M. Jones, *J. Chem. Phys.*, 1966, **45**, 3449–3450.

7 D. H. Parker and R. B. Bernstein, *Ann. Rev. Phys. Chem.*, 1989, **40**, 561.

8 D. H. Parker, K. K. Chakravorty and R. B. Bernstein, *J. Phys. Chem.*, 1981, **85**, 466.

9 R. N. Zare, *Annual Review of Analytical Chemistry*, 2012, **5**, 1–14.

10 S. Y. T. van de Meerakker, H. L. Bethlem, N. Vanhaecke and G. Meijer, *Chemical Reviews*, 2012, **112**, 4828–4878.

11 D. W. Chandler and P. L. Houston, *J. Chem. Phys.*, 1987, **87**, 1445–1447.

12 A. T. J. B. Eppink and D. H. Parker, *Rev. Sci. Instrum.*, 1997, **68**, 3477–3484.

13 K. H. Kramer and R. B. Bernstein, *J. Chem. Phys*, 1965, **42**, 767.

14 M. C. van Beek, J. J. ter Meulen and M. H. Alexander, *J. Chem. Phys.*, 2000, **113**, 628.

15 D. W. Chandler and S. Stolte, Chapter 5, *Tutorials in Molecular Reaction Dynamics,* Eds., M. Brouard and C. Vallance, Royal Society of Chemistry, Cambridge, UK, 2010.

16 C. J. Eyles, M. Brouard, C.-H. Yang, J. Kłos, F. J. Aoiz, A. Gijsbertsen, A. E. Wiskerke and S. Stolte, *Nat. Chem.*, 2011, **3**, 597.

17 J. Kłos, F. J. Aoiz, J. E. Verdasco, M. Brouard, S. Marinakis and S. Stolte, *J. Chem. Phys.*, 2007, **127**, 031102.

18 G. Sarma, S. Marinakis, J. J. ter Meulen, D. H. Parker and K. G. McKendrick, *Nat. Chem.*, 2012, **4**, 985.

19 D. Watanabe, H. Ohoyama, T. Matsumura and T. Kasai, *Phys. Rev. Lett.*, 2007, **99**, 043201.

20 Y.-P. Chang, K. Długołęcki, J. Küpper, D. Rösch, D. Wild and S. Willitsch, *Science*, 2013, **342**, 98–101.

21 M. C. van Beek, G. Berden, H. L. Bethlem and J. J. ter Meulen, *Phys. Rev. Lett.*, 2001, **86**, 4001.

22 M. C. van Beek, J. J. ter Meulen and M. H. Alexander, *J. Chem. Phys.*, 2000, **113**, 637.

23 M. J. L. de Lange, M. Drabbels, P. T. Griffiths, J. Bulthuis,

S. Stolte and J. G. Snijders, *Chem. Phys. Lett.*, 1999, **313**, 491.

24 M. H. Alexander and S. Stolte, *J. Chem. Phys.*, 2000, **112**, 8017.

25 P.-Y. Tsai, D.-C. Che, M. Nakamura, K.-C. Lin and T. Kasai, *Phys. Chem. Chem. Phys.*, 2011, **13**, 1419–1423.

26 B. Friedrich and D. R. Herschbach, *Nature*, 1991, **353**, 412.

27 H.-J. Loesch and A. Remscheid, *J. Chem. Phys.*, 1990, **93**, 4779.

28 F. Wang, K. Liu and T. P. Rakitzis, *Nat. Chem.*, 2012, **4**, 636–641.

29 H. Stapelfeldt and T. Seideman, *Rev. Mod. Phys.*, 2003, **75**, 543.

30 G. Paterson, M. L. Costen and K. G. McKendrick, *Int. Rev. Phys. Chem.*, 2012, **31**, 69.

31 H. Chadwick, M. Brouard, T. Perkins and F. J. Aoiz, *Int. Rev. Phys. Chem.*, 2014, **33**, 79.

32 S.-M. Wu, D. C. Radenovic, W. J. van der Zande, G. C. Groenenboom, D. H. Parker, C. Vallance and R. N. Zare, *Nat. Chem.*, 2011, **3**, 28.

33 H. L. Bethlem, G. Berden and G. Meijer, *Phys. Rev. Lett.*, 1999, **83**, 1558–1561.

34 J. J. Gilijamse, S. Hoekstra, S. Y. T. van de Meerakker, G. C. Groenenboom and G. Meijer, *Science*, 2006, **313**, 1617–1620.

35 L. Scharfenberg, J. Kłos, P. J. Dagdigian, M. H. Alexander, G. Meijer and S. Y. T. van de Meerakker, *Phys. Chem. Chem. Phys.*, 2010, **12**, 10660.

36 M. Kirste, X. Wang, H. C. Schewe, G. Meijer, K. Liu, A. van der Avoird, L. M. C. Janssen, K. B. Gubbels, G. C. Groenenboom and S. Y. T. van de Meerakker, *Science*, 2012, **338**, 1060–1063.

37 A. von Zastrow, J. Onvlee, S. N. Vogels, G. C. Groenenboom, A. van der Avoird and S. Y. T. van de Meerakker, *Nat. Chem.*, 2014, **6**, 216–221.

38 E. Narevicius and M. G. Raizen, *Chem. Rev.*, 2012, **112**, 4879–4889.

39 L. D. Carr, D. DeMille, R. V. Krems and J. Ye, *New J. of Phys.*, 2009, **11**, 055049.

40 B. C. Sawyer, B. K. Stuhl, D. Wang, M. Yeo and J. Ye, *Phys. Rev. Lett.*, 2008, **101**, 203203.

41 B. C. Sawyer, B. K. Stuhl, M. Yeo, T. V. Tscherbul, M. T. Hummon, Y. Xia, J. Klos, D. Patterson, J. M. Doyle and J. Ye, *Phys. Chem. Chem. Phys.*, 2011, **13**, 19059–19066.

42 S. Willitsch, M. T. Bell, A. D. Gingell, S. R. Procter and T. P. Softley, *Phys. Rev. Lett.*, 2008, **100**, 043203.

43 M. T. Bell, A. D. Gingell, J. M. Oldham, T. P. Softley and S. Willitsch, *Faraday Discuss.*, 2009, **142**, 73–91.

44 L. P. Parazzoli, N. J. Fitch, P. S. Żuchowski, J. M. Hut-

son and H. J. Lewandowski, *Phys. Rev. Lett.*, 2011, **106**, 193201.

45 B. K. Stuhl, M. T. Hummon, M. Yeo, G. Quéméner, B. J. L. and J. Ye, *Nature*, 2012, **492**, 396–400.

46 M. T. Hummon, T. V. Tscherbul, J. Klos, H.-I. Lu, E. Tsikata, W. C. Campbell, A. Dalgarno and J. M. Doyle, *Phys. Rev. Lett.*, 2011, **106**, 053201.

47 S. Chefdeville, Y. Kalugina, S. Y. T. van de Meerakker, C. Naulin, F. Lique and M. Costes, *Science*, 2013, **341**, 1094–1096.

48 A. B. Henson, S. Gersten, Y. Shagam, J. Narevicius and E. Narevicius, *Science*, 2012, **338**, 234–238.

49 E. Lavert-Ofir, Y. Shagam, A. B. Henson, S. Gersten, J. Kłos, P. S. Żuchowski, J. Narevicius and E. Narevicius, *Nat. Chem.*, 2014, **6**, 332–335.

50 B. Bertsche, J. Jankunas and A. Osterwalder, *CHIMIA International Journal for Chemistry*, 2014, **68**, 256–259.